Ternary polymer solar cells with iridium-based polymer PM6Ir1 as donor and N3:ITIC-Th as acceptors exhibiting over 17.2% efficiency

Shuping Zhang[a], Miao Zhang[a,c], Xuelin Wang[a], Chunyu Xu[a], Wenjing Xu[a], Jinhua Gao[a]*, Jian Wang[b], Wai-Yeung Wong[c,d]*, Jae Hoon Son[e], Sang Young Jeong[e], Han Young Woo[e], Fujun Zhang[a]*

a) School of Science, Beijing Jiaotong University, 100044, Beijing, China.

b) College of Physics and Electronic Engineering, Taishan University, 271021, Taian, China.

c) Department of Applied Biology and Chemical Technology and Research Institute for Smart Energy, The Hong Kong Polytechnic University, Hung Hom, Hong Kong, China.

d) The Hong Kong Polytechnic University Shenzhen Research Institute, 518057, Shenzhen, China.

e) Organic Optoelectronic Materials Laboratory, Department of Chemistry, College of Science, Korea University, 02841, Seoul, Republic of Korea.

Corresponding Email:

E-mail: jinhuagao@bjtu.edu.cn (JH), wai-yeung.wong@polyu.edu.hk (WY), fjzhang@bjtu.edu.cn (FJ)

Abstract

Iridium-based polymer PM6Ir1 as electron donor and two nonfullerene materials N3 and ITIC-Th as electron acceptors were selected to prepare efficient polymer solar cells (PSCs). ITIC-Th was used as the third component to enhance photon harvesting and morphology regulator to optimize molecular arrangement and phase separation in the ternary active layer. The improvement in open circuit voltage (0.86 V vs. 0.84 V), short circuit current density (26.53 mA cm^{-2} vs. 26.13 mA cm^{-2}) and fill factor (75.47% vs. 74.11%) are simultaneously obtained for the PSCs with 10 wt% of ITIC-Th in the acceptor mixture, leading to the power conversion efficiency (PCE) enhancement from 16.27% to 17.22%. The charge mobility and charge transport balance in the ternary

active layer can be enhanced by incorporating ITIC-Th, resulting from the optimzed phase separation and molecular arrangement with ITIC-Th as morphology regulator. The positive effect of ITIC-Th incorporation on PCE improvement can be demonstrated from the relatively high external quantum efficiency values in the spectral range from 300 to 820 nm of the optimal ternary PSCs.

Keywords: Iridium-based polymer; Nonfullerene acceptor; Morphology regulator; Power conversion efficiency

Introduction

As the next generation of photovoltaic devices with great development prospects, polymer solar cells (PSCs) have gradually aroused extensive concern on account of their special characteristics such as light-weight, easy processing, semitransparency and flexibility.[1-3] Over the last few years, PSCs have achieved remarkable progress with new photovoltaic materials and device engineering.[4-7] From the materials perspective, most work focused on non-fullerene materials with different halogen substitution, side-chain engineering, fused-ring core and end groups engineering, such as ITIC, Y6 and their derivatives.[8-11] Tao et al. introduced low concentrations of iridium or platinum complexes to the famous donor polymer of PTB7 or PTB7-Th backbone, leading to the PCE improvement of the PSCs, suggesting that incorporation of iridium or platinum atom in the commonly used polymer donors should be an extra efficient approach to improve the PCE of PSCs.[12-14] Peng et al. proposed a strategy of platinum(II) complexation to regulate the molecular packing and crystallinity of polymer donors, optimize the active layer morphology, and elevate the power conversion efficiency (PCE) of the corresponding PSCs.[15] Min et al. exploited a sequence of polymer donors by incorporating different content of iridium (Ir) complexes into PM6 conjugated backbone.[16] Compared with PM6:Y6 based PSCs, one of the Iridium-based polymer donor PM6Ir1, exhibits marked enhancement in PCE when blending with Y6, resulting from the optimized packing order and charge mobility of PM6Ir1 in the blend systems.[17] Based on the well optimized binary blend systems with one donor and one acceptor, there is still a significant room to improve PCE of PSCs by adding a third component.[18-21] The appropriate third component serves multiple functions in

improving the performance of PSCs, such as enhancing the efficiency of photon harvesting, minimizing the energy loss, optimizing the molecular arrangement and phase separation morphology in the ternary blend system.[22-24] The selection of the third component always obeys the principles of the complementary photon harvesting, good compatibility of materials used, as well as the complementary photovoltaic parameters of the corresponding binary devices.[25, 26] Although there is a large amount of work on ternary PSCs based on two donors or two acceptors, there is few report on the preparation of ternary PSCs employing iridium or platinum-based polymer donors. Here, the typical works on iridium or platinum-based polymer donors for achieving efficient PSCs are summarized in **Table 1**. It is apparent that the iridium or platinum-based polymers play a positive effect in improving PCE of binary PSCs. Ternary strategy should have great potential in further enhancing PCE of PSCs with iridium or platinum-based polymer as donor.

Table 1 Recent progress of PSCs with iridium or platinum-based polymer as donor.

Active Layer	J_{SC} (mA cm^{-2})	V_{OC} (V)	FF (%)	PCE (%)	Reference
PTB7Ir1:PC_{71} BM	18.14	0.750	64.00	8.71	12
PTB7Ir2.5:PC_{71} BM	17.86	0.750	60.00	8.04	
PTB7-ThPt1:PC_{71} BM	15.11	0.810	67.76	8.31	13
PTB7-ThPt1.5:PC_{71} BM	16.21	0.800	65.01	8.45	
PTB7-ThPt5:PC_{71} BM	13.50	0.810	66.21	7.24	
PTB7-ThIr0.5:PC_{71} BM	15.88	0.800	66.07	8.38	14
PTB7-ThIr1:PC_{71} BM	16.60	0.800	69.36	9.19	
PTB7-ThIr1.5:PC_{71} BM	15.00	0.800	69.34	8.30	
Pt5:Y6	25.89	0.800	72.70	15.06	15
Pt10:Y6	26.45	0.810	76.30	16.35	
Pt15:Y6	26.02	0.820	73.90	15.77	
PM6:Y6-C2	25.65	0.840	73.01	15.73	16
PM6-Ir1.5:Y6-C2	26.09	0.839	77.98	17.09	
PM6-Ir0.5:Y6	26.28	0.845	74.02	16.44	17
PM6-Ir1:Y6	26.15	0.845	78.40	17.32	
PM6-Ir2.5:Y6	26.07	0.847	74.15	16.37	
PM6-Ir5:Y6	25.92	0.842	73.43	16.03	
PM6Ir1:N3	26.13	0.840	74.11	16.27	This work
PM6Ir1:N3:ITIC-Th	26.53	0.860	75.47	17.22	

In this work, a sequence of ternary PSCs were prepared with iridium-based polymer PM6Ir1 as donor, ITIC-Th and N3 as acceptors. The chemical structures of the materials used and the device architecture are displayed in **Fig. 1a**. The highest occupied molecular orbital (HOMO) and the lowest unoccupied molecular orbital

(LUMO) of PM6Ir1, ITIC-Th and N3 are presented in **Fig. 1b**. The cascaded energy levels can offer more potential avenues for charge transfer and charge transport in the ternary blend system. The normalized absorption spectra of neat films is depicted in **Fig. 1c**. The neat PM6Ir1, ITIC-Th and N3 films have obvious absorption peaks at about 620, 680 and 830 nm, respectively. The absorption spectra of blend films with different ITIC-Th content were measured, as depicted in **Fig. S2**. The photon harvesting of ternary blend films in the spectral range from 580 nm to 740 nm can be gradually increased along with ITIC-Th content increment. Meanwhile, photon harvesting of ternary blend films in long wavelength range is gradually decreased, which can be well explained from the absorption spectrum of the neat N3 and ITIC-Th films. The photon harvesting of ternary blend films should be optimized by balancing the enhanced photon harvesting in 580 nm to 740 nm spectral range and the decreased photon harvesting in long wavelength range. The PCE of binary PM6Ir1:N3 devices reaches to 16.27%, which is slightly higher than the formerly reported 15.98% of PM6:N3 based PSCs[11], indicating that the introduction of iridium complex into the backbone of PM6 can lead to the performance enhancement of devices. The binary PM6Ir1:ITIC-Th devices achieve a PCE of 10.39%, which exhibits complementary photovoltaic parameters in comparison with the binary PM6Ir1:N3 device. The PCE of optimal ternary devices reaches up to 17.22% by integrating the superiorities of two binary devices in photovoltaic parameters, resulting from the simultaneous elevated short circuit current density (J_{SC}) of 26.53 mA cm^{-2}, open circuit voltage (V_{OC}) of 0.86 V and fill factor (FF) of 75.47% in contrast with the binary PM6Ir1:N3 device with a PCE of 16.27%. The J_{SC} and FF improvement of the ternary devices should be attributed to the improved photon harvesting, exciton dissociation and charge transport in ternary blend system. The energy-loss (E_{loss}) of optimal ternary devices is reduced by incorporating appropriate ITIC-Th, contributing to the V_{OC} enhancement of the ternary devices.

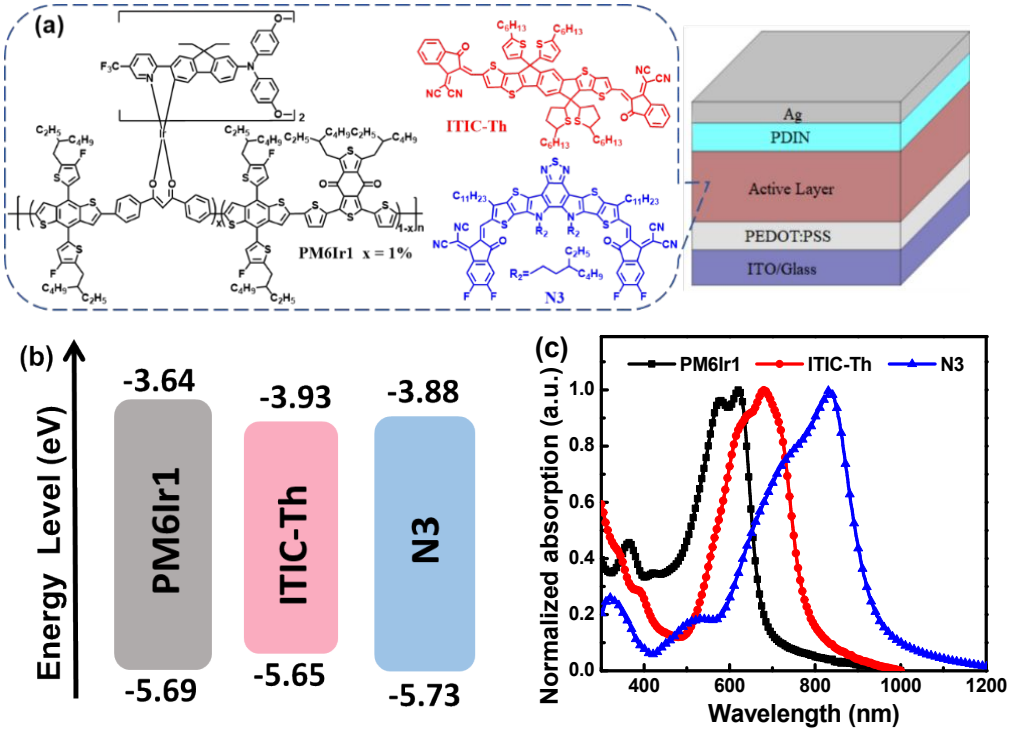

Fig. 1 (a) Chemical structures of PM6Ir1, ITIC-Th and N3 and device architecture (b) Energy levels of used materials. (c) Normalized absorption spectra of used materials.

Results and discussion

A sequence of binary and ternary PSCs were fabricated with a conventional architecture of ITO/PEDOT:PSS/Active layer/PDIN/Ag, and the current-density versus voltage (*J-V*) curves of all PSCs were measured under AM 1.5G (100 mW cm^{-2} light intensity), as presented in **Fig. 2a**. On the basis of the *J-V* characteristic curves, the detailed photovoltaic parameters of related devices are presented in **Table 2** The binary PM6Ir1:ITIC-Th devices acquire a PCE of 10.39%, along with a J_{SC} of 15.32 mA cm^{-2}, a V_{OC} of 0.96 V and a FF of 68.23%. The PCE of binary PM6Ir1:N3 devices reaches to 16.27% with a J_{SC} of 26.13 mA cm^{-2}, a V_{OC} of 0.84 V and a FF of 74.11%. The V_{OC} of the binary PM6Ir1:ITIC-Th devices is higher than that of the binary PM6Ir1:N3 devices, and the J_{SC} and FF of the binary PM6Ir1:N3 devices are appreciably higher than those of the binary PM6Ir1:ITIC-Th devices. The preponderances of two kinds of PSCs in photovoltaic parameters may be integrated into the ternary PSCs by using ITIC-Th:N3 as acceptor. The J_{SC}s and FFs of optimal ternary devices are slightly raised and then reduced in the wake of ITIC-Th content increment in the ternary blend system,

while the V_{OC}s of ternary devices are gradually raised as more ITIC-Th is added. A PCE of 17.22% is acquired in the optimized ternary devices with 10 wt% of ITIC-Th in the acceptor mixture, ascribing to the simultaneous enhancement of J_{SC} (26.53 mA cm^{-2}), V_{OC} (0.86 V), and FF (75.47%) in contrast with the binary PM6Ir1:N3 devices.

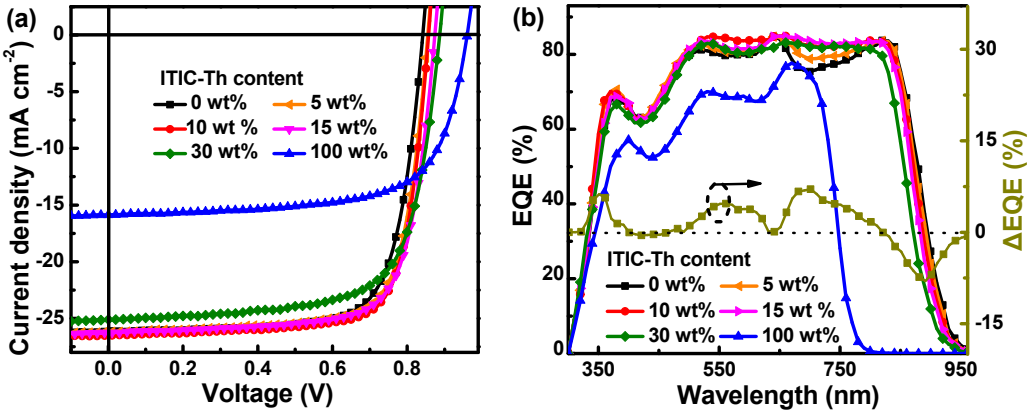

Fig. 2 (a) *J*–*V* curves. (b) EQE spectra of all PSCs with different ITIC-Th content and ΔEQE spectra between the optimal ternary PSCs and the N3-based binary PSCs.

Table 2 Key photovoltaic parameters of all PSCs with different ITIC-Th content.

ITIC-Th	J_{SC}	*Calc.* J_{SC}	V_{OC}	FF	PCE (Ave. ± Dev.)[a]	E_{loss}	R_S	R_{SH}
(wt%)	(mA cm^{-2})	(mA cm^{-2})	(V)	(%)	(%)	(eV)	(Ω cm^2)	(Ω cm^2)
0	26.13	25.24	0.84	74.11	16.27 (16.18 ± 0.09)	0.573	2.4	740.7
5	26.22	25.48	0.85	75.30	16.78 (16.67 ± 0.12)	0.562	2.3	806.5
10	26.53	25.71	0.86	75.47	17.22 (17.12 ± 0.11)	0.561	2.2	869.3
15	26.28	25.40	0.87	74.14	16.95 (16.83 ± 0.13)	0.565	2.4	775.2
30	25.11	24.43	0.89	69.74	15.59 (15.51 ± 0.09)	0.568	2.8	719.4
100	15.87	15.55	0.96	68.23	10.39 (10.32 ± 0.08)	0.738	3.2	575.7

[a]The average (Ave.) and deviations (Dev.) of PCEs were calculated from ten individual cells.

To investigate the influence of introducing ITIC-Th for boosting the performance of ternary devices, the dependence of the detailed energy-loss (E_{loss}) of PSCs on ITIC-Th content was studied. The E_{loss} of PSCs can be reckoned by using the formula: $E_{loss} = E_g - eV_{OC}$, where E_g can be determined on the grounds of the intersection point of the normalized absorption and emission spectra of the acceptors, as presented in **Fig. S3**.[27-29] The E_{loss}s of ternary PSCs decrease at first and then increase in the wake of the increment of ITIC-Th proportion in the ternary blend system. The E_{loss} of optimized

ternary devices is 0.561 eV, which is lower than 0.573 eV for binary PM6Ir1:N3 devices and 0.738 eV for the binary PM6Ir1:ITIC-Th devices. The reduced E_{loss} of optimal ternary device should take a significant part in the performance improvement. To better understand FF variation of ternary PSCs dependence on ITIC-Th content in acceptors, the series resistance (R_S) and shunt resistance (R_{SH}) were calculated according to *J-V* curves of PSCs, as summarized in Table 2. The R_S values of PSCs show a decreased and then increased trend along with the increase of ITIC-Th content, and the R_{SH} values of PSCs exhibit an opposite trend compared with that of R_S values. The minimum R_S of 2.2 Ω cm^2 and maximum R_{SH} of 869.3 Ω cm^2 were simultaneously obtained for the PSCs with 10 wt% ITIC-Th in acceptors, which is responsible for the highest FF of the optimal ternary PSCs. To further clarify the effect of ITIC-Th content on the performance of ternary PSCs, the external quantum efficiency (EQE) spectra of all devices were measured, as exhibited in **Fig. 2b**. In the wavelength range of 300~820 nm, the EQE values of optimal ternary devices are higher than that of binary PM6Ir1:N3 spectral difference (ΔEQE) between ternary blend system and binary PM6Ir1:N3 devices. The positive ΔEQE values in the region of 300-820 nm ought to be largely ascribed to the better phase-separated morphology in favor of effective charge separation and transport in the ternary blend system, in accordance with the considerable FF (75.47%) of the optimal ternary devices.

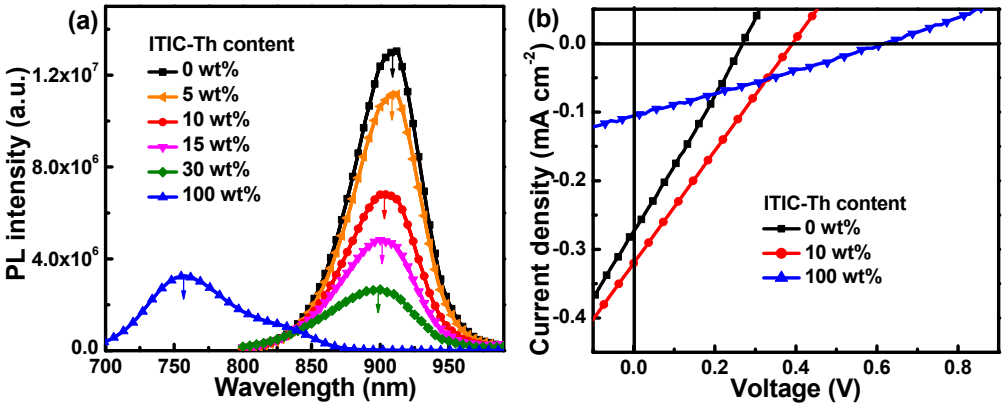

Fig. 3 (a) PL spectra of neat N3, ITIC-Th and their blend films. (b) *J-V* curves of cells with N3, ITIC-Th or N3:ITIC-Th as active layers under one sun light illumination.

To clarify the charge or exciton dynamic process between ITIC-Th and N3, photoluminescence (PL) spectra of neat and blend films were investigated under 680

nm light excitation and shown in **Fig. 3a**. Neat ITIC-Th films exhibit relatively weak and wide PL emission with an emission peak at 760 nm. The strong PL emission of the neat N3 films can be clearly observed from its PL spectra with an emission peak at 900 nm. The PL emission of N3 in blend films is gradually quenched by increasing the ITIC-Th content, suggesting the presence of efficient charge transfer between ITIC-Th and N3. To further confirm charge transfer between ITIC-Th and N3, a sequence of devices were fabricated with ITIC-Th, N3 and ITIC-Th:N3 as the active layer without PM6Ir1. The *J-V* characteristic curves of devices under one sun light illumination are displayed in **Fig. 3b**. The J_{SC} of specific cells with ITIC-Th:N3 as active blend layer is larger than that of the specific cells with ITIC-Th or N3 as the active blend layer, further implying the charge transfer from ITIC-Th to N3. The charge transfer between ITIC-Th and N3 provides another channel for exciton dissociation in the ternary blend system, which agrees well with the J_{SC} enhancement of the ternary device.

To further understand the process of light harvesting absorption, exciton dissociation and carrier transport/recombination in the blend system, photocurrent density (J_{ph}) versus effective bias voltage (V_{eff}) characteristics of typical PSCs were measured and are displayed in **Fig. 4a**. Assuming that all generated electron-hole pairs fully dissociated into free charges and are swept out under high V_{eff} condition, the J_{ph} can be defined as the saturated current density (J_{sat}).[30, 31] The J_{sat} values are 27.64, 27.84 and 17.35 mA cm^{-2} for binary PM6Ir1:N3 devices, optimal ternary devices and binary PM6Ir1:ITIC-Th devices, respectively. The J_{sat} value of the optimal ternary PSCs is relatively large, implying photon capture enhancement in the optimized ternary active layers. The exciton dissociation efficiency (η_{diss}) and charge collection efficiency (η_{coll}) can be assessed on the basis of the equations of $\eta_{diss} = J_{ph}^{*}/J_{sat}$ and $\eta_{coll} = J_{ph}^{\#}/J_{sat}$, the J_{ph}^{*} and $J_{ph}^{\#}$ refer to the J_{ph} under short-circuit condition and maximal-power-output condition, respectively.[32-34] The detailed values of (J_{phs}, η_{diss} and η_{coll}) of the typical PSCs are presented in **Table S1**. The η_{diss} and η_{coll} values are 94.55% and 86.24%, 95.28% and 87.47%, 91.47% and 77.69% for binary PM6Ir1:N3 devices, optimal ternary devices and binary PM6Ir1:ITIC-Th devices, respectively. The simultaneously elevated η_{diss} and η_{coll} values of ternary blend system should be ascribed to the well optimized

phase separation by adding appropriate ITIC-Th as the morphology regulator.

The *J–V* curves of typical devices were tested under AM 1.5G illumination with varying incident light intensity (P_{light}) to elucidate the charge recombination behavior in blend system, as presented in **Fig. S4**. In accordance with the corresponding *J–V* curves, the V_{OC}s and J_{SC}s of the typical PSCs versus the P_{light} are plotted in **Fig. 4b**. The relationship of J_{SC} and P_{light} can be defined as: $J_{SC} \propto P_{light}^{\alpha}$.[33] The exponential factor α refers to the extent of bimolecular recombination. If the bimolecular recombination is thoroughly inhibited in the active layer, J_{SC} has a linear dependence on P_{light}, with α value equal to 1. The α value of ternary blend system was 0.957, which was higher than that of the two binary devices (0.941 and 0.946), implying that the bimolecular recombination can be efficiently inhibited with a small amount of ITIC-Th incorporation. The correlation between V_{OC} and P_{light} can be represented as: $V_{OC} \propto \beta(KT/q)$ ln (P_{light}), where *K, T* and *q* represent the Boltzmann constant, absolute temperature, and elementary charge, respectively.[36-38] The trap-assisted recombination in the active layer will be overlooked if the β value is close to 1.[39, 40] The β of 1.282 for the optimal ternary devices was closer to 1 than that of 1.441 for the binary PM6Ir1:N3 device and 1.319 for the binary PM6Ir1:ITIC-Th device, implying the efficiently weakened trap-assisted recombination in the ternary blend system. The synchronously mitigated bimolecular and trap-assisted recombination are in favor of charge transport and collection, as confirmed from the improved FF of 75.47% in the optimal ternary PSCs.

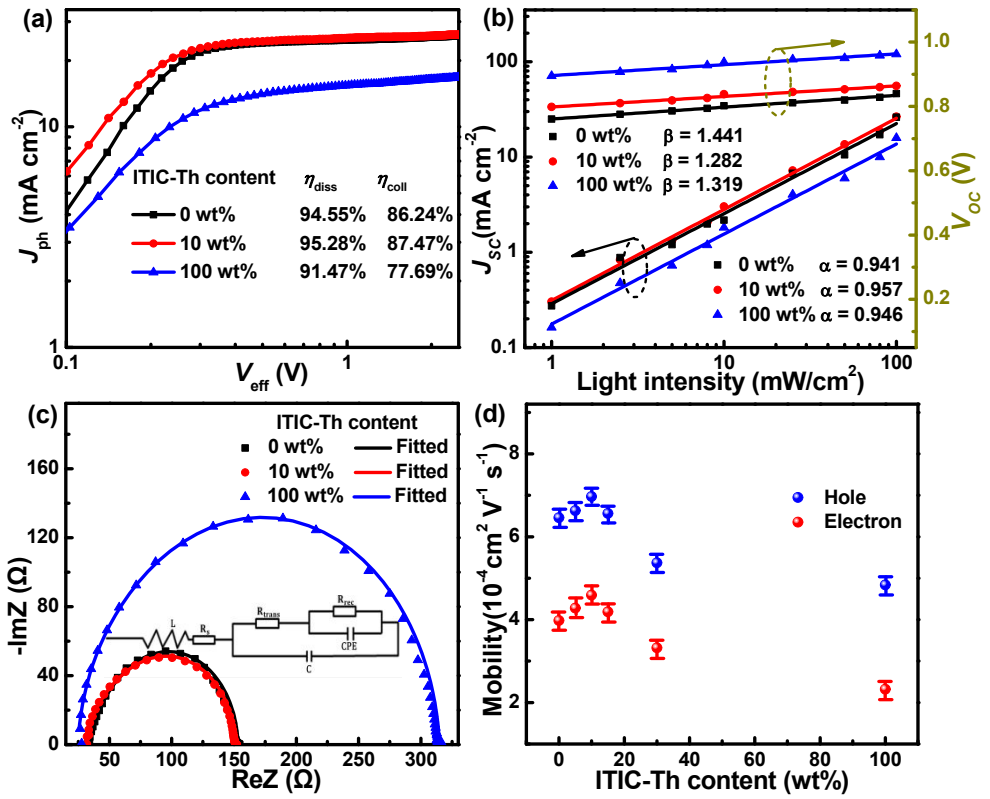

Fig. 4 The typical PSCs (a) J_{ph}-V_{eff} curves. (b) J_{SC} versus light intensity and V_{OC} versus light intensity. (c) Nyquist plots and equivalent circuit. (d) Charge mobility in blend films with different ITIC-Th content.

To gain in-depth investigation of the effect of ITIC-Th content on electron transport and recombination process, electrochemical impedance spectroscopy (EIS) in blend systems were performed over the frequency range of 5 Hz~5 MHz under $V = V_{OC}$s of the corresponding PSCs to eliminate the direct current of the devices.[41] **Fig. 4c** exhibits the Nyquist plots of the typical PSCs, and the insert displays the corresponding simplified circuit model for fitting the Nyquist plots data. The inductance (L) is adopted to nullify the effect of connecting wires under the high frequency scanning. R_s is the series resistance induced by the electrode and bulk resistance in the blend systems. R_{trans} and R_{rec} are defined as the transport resistances and recombination resistances in the devices, respectively.[42-45] The capacitor (C) describes the dielectric properties of PSCs.[46] A capacitance-like constant phase element (CPE) indicates the nonideal behavior of the capacitor. The CPE is determined by capacitance value (CPE_T) and inhomogeneous constant (CPE_P) between 0 and 1, as well as angular frequency (ω),

expressed as $Z = (CPE_T)^{-1} (i\omega)^{CPE_P}$.[47, 48] If the CPE_P value approaches to 1, then the CPE is equivalent to an ideal capacitor without any defects or grain boundaries at the donor:acceptor interface.[49] The corresponding parameters on the basis of simplified circuit model are summarized in **Table S2**. The binary PM6Ir1:ITIC-Th device has a relatively large R_{trans} value of 189 Ω, in accordance with the fairly low FF(68.23%). The R_{trans} values are decreased from 59.5 Ω for binary PM6Ir1:N3 device to 54.9 Ω for the optimal ternary device, while the R_{rec} values are elevated from 62.4 Ω for binary PM6Ir1:N3 device to 65.9 Ω for the optimal ternary device. The lower R_{trans} and higher R_{rec} of the ternary PSCs imply that the proper amount ITIC-Th introduced can promote electron transport and inhibit charge recombination in ternary blend system, facilitating the improvement of FF for ternary devices. The values of CPE_P are 0.910, 0.955 and 0.859 for binary PM6Ir1:N3 device, ternary blend system and binary PM6Ir1:ITIC-Th device, respectively. The CPE_P of the ternary devices come near 1 compared with that of binary PSCs, indicating that the interface capacitance is more electrically ideal after adding appropriatde ITIC-Th in the blend systems.

The space-charge limiting curve (SCLC) measurement was exploited to characterize the exciton transportation in the blend systems. **Fig. S5** depicts the $\ln(Jd^3/V^2)$-$(V/d)^{0.5}$ characteristic curves of hole-only and electron-only devices. The detailed hole (μ_h) and electron mobility (μ_e) of the related devices are presented in **Table S3**. The dependence of μ_h and μ_e values toward the increment of ITIC-Th proportion in the ternary blend system is plotted in **Fig. 4d**. With an increase of the ITIC-Th content, both μ_h and μ_e of the blend system exhibit a trend of increasing first and then decreasing. The μ_h and μ_e values of the optimal ternary devices are enhanced to 6.97×10^{-4} and 4.59×10^{-4} $cm^2 V^{-1} s^{-1}$ respectively, indicating that the exciton transportation channel could be optimized with the introduction of a small amount of ITIC-Th. The ratios of μ_h/μ_e can be employed to assess the balance of hole and electron transport.[50-52] The μ_h/μ_e ratios are 1.52, 1.62 and 2.08 for the optimal ternary and two binary active layers, indicating the adequately balanced exciton transportation in the optimized ternary blending system. The increased mobility of charges and more balanced μ_h/μ_e ratios play a significant part in promoting charge extraction and inhibiting charge recombination, in accordance with

the higher FFs of the ternary blend system with appropriate ITIC-Th incorporation.

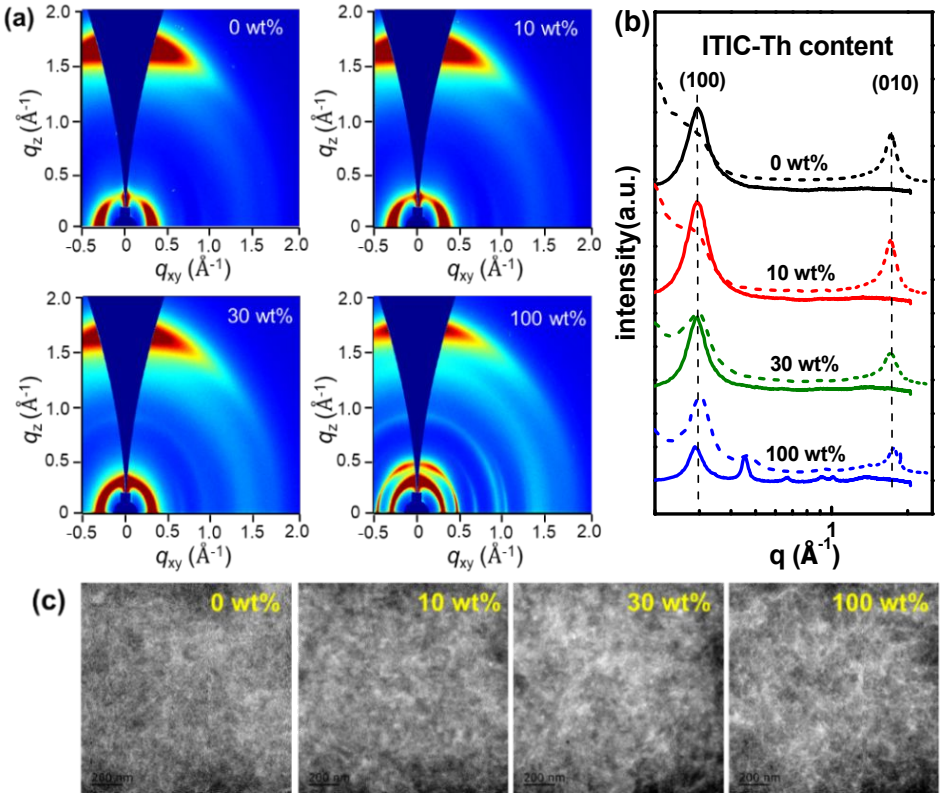

.**Fig. 5** (a) 2D-GIWAXS patterns of blend films with various ITIC-Th content. (b) In-plane (solid lines) and out-of-plane (dotted lines) line-cut profiles of GIWAXS. (c) TEM images of corresponding blend films.

The two-dimensional grazing incidence wide angle X-ray scattering (2D-GIWAXS) patterns were studied to further acquire the molecular packing behaviors in the devices. **Fig. 5a** and **5b** show the 2D-GIWAXS patterns and the related intensity profiles along in-plane(IP) and out-of-plane (OOP) directions of the blend films, respectively. The PM6Ir1:N3 blend films present IP (100) diffraction peak and OOP (010) diffraction peak, implying that the blend films had a preferential face-on molecular orientation. The relatively weak IP (100), (200) as well as OOP (010) diffraction peaks were seen on the binary PM6Ir1:ITIC-Th device. Meanwhile, the OOP (100) diffraction peak was seen on the binary PM6Ir1:ITIC-Th device, implying the presence of face-on and edge-on molecular orientation in blend films.[53, 54] In the optimal ternary blend system, the intensities of IP (100) and OOP (010) diffraction peaks were synchronized enhanced, indicating the more face-on molecular orientation in ternary blend films, which is conducive to charge transport along with the normal direction of substrate. To further

analyze the influence of the incorporation of ITIC-Th on the film morphologies of the PSCs, transmission electron microscopy (TEM) measurements of blend films were characterized as displayed in **Fig. 5c**. The homogeneous structures were seen on the TEM images in binary PM6Ir1:N3 device. The considerable bright regions can be seen on the TEM image of the binary PM6Ir1:ITIC-Th device, leading to enlarged phase separation with a lack of the donor/acceptor interfaces for exciton dissociation and electron transport.[55, 56] After adding more ITIC-Th, the TEM image of the ternary blend system showed gradually altered morphology and pronounced phase separation, implying that ITIC-Th can be employed as the morphology regulator. The better phase-separated morphology could be formed in favor of efficient exciton dissociation and electron transport in the ternary blend system with proper ITIC-Th incorporation, which can be confirmed from the simultaneous enhancement of J_{SC} and FF in the optimal ternary devices.

Conclusion:

In this work, iridium-based polymer PM6Ir1 was selected as donor and two nonfullerene materials N3 and ITIC-Th were selected as acceptor to prepare ternary PSCs. The PCE of the ternary devices reach 17.22% with 10 wt% of ITIC-Th in the acceptors mixture, attributing to the simultaneous enhanced V_{OC} of 0.86 V, J_{SC} of 26.53 mA cm^{-2} and FF of 75.47% with respect to the binary PM6Ir1:N3 device with a PCE of 16.27%. According to the experimental results of EIS, SCLC, 2D-GIWAXS and TEM, molecular arrangement, charge mobility and phase separation morphology of the ternary blend systems can be well modulated via adding appropriate ITIC-Th as the morphology regulator. By employing ternary strategy based on efficient binary PSCs while maintaining simple cell manufacturing technology, over 5% PCE increase can be acquired. Ternary strategy should show a huge promise in fabricating large scale efficient PSCs.

Conflicts of interest

The authors declare no conflict of interest.

Acknowledgements

S. Z. and M. Z. made equal contributions to this work. This work is financially

supported by the National Natural Science Foundation of China (61975006, 62175011, 52073242), Beijing Natural Science Foundation (4192049), the Science, Technology and Innovation Committee of Shenzhen Municipality (JCYJ20180507183413211), the Hong Kong Research Grants Council (PolyU 153058/19P and C5037-18G), Hong Kong Polytechnic University (1-ZE1C), Research Institute for Smart Energy (CDA2), Ms. Clarea Au for the Endowed Professorship in Energy (847S).

Author Contributions

S. Zhang carried out the device fabrication and characterization. M. Zhang synthesized the materials PM6Ir1. F. Zhang, J. Gao and W.-Y. Wong designed the experiments and finished the manuscript writing. X. Wang, C. Xu and W. Xu also took part in the experimental details. S. Zhang, J. Son, S. Jeong and H. Woo carried out the GIWAXS experiment. S. Zhang and J. Wang finished the impedance spectroscopy measurement and analysis. All authors discussed and commented on the paper.

Reference

1. M. Yao, T. Li, Y. Long, P. Shen, G. Wang, C. Li, J. Liu, W. Guo, Y. Wang, L. Shen and X. Zhan, *Sci. Bull.,* 2020, **65**, 217-224.
2. Y. Li and Y. Zou, *Adv. Mater.,* 2008, **20**, 2952-2958.
3. H. Kang, G. Kim, J. Kim, S. Kwon, H. Kim and K. Lee, *Adv. Mater.*, 2016, **28**, 7821-7861.
4. X. Gong, M. Tong, F. G. Brunetti, J. Seo, Y. Sun, D. Moses, F. Wudl and A. J. Heeger, *Adv. Mater.*, 2011, **23**, 2272-2277.
5. D. Qian, Z. Zheng, H. Yao, W. Tress, T. R. Hopper, S. Chen, S. Li, J. Liu, S. Chen, J. Zhang, X. K. Liu, B. Gao, L. Ouyang, Y. Jin, G. Pozina, I. A. Buyanova, W. M. Chen, O. Inganas, V. Coropceanu, J. L. Bredas, H. Yan, J. Hou, F. Zhang, A. A. Bakulin and F. Gao, *Nat. Mater.*, 2018, **17**, 703-709.
6. C. Xu, K. Jin, Z. Xiao, Z. Zhao, X. Ma, X. Wang, J. Li, W. Xu, S. Zhang, L. Ding, F. Zhang, *Adv. Funct. Mater.*, 2021, **31**, 2107567.

7. P. Bi, T. Xiao, X. Yang, M. Niu, Z. Wen, K. Zhang, W. Qin, S. K. So, G. Lu, X. Hao and H. Liu, *Nano Energy*, 2018, **46**, 81-90.

8. K. Jiang, Q. Wei, J. Y. L. Lai, Z. Peng, H. K. Kim, J. Yuan, L. Ye, H. Ade, Y. Zou and H. Yan, *Joule*, 2019, **3**, 3020-3033.

9. T. Chen, K. Peng, Y. Lin, Y. Su, K. Ma, L. Hong, C. Chang, J. Hou, C. Hsu, *J. Mater. Chem. A*, 2020, **8**, 1131-1137.

10. J. Yuan, Y. Zhang, L. Zhou, G. Zhang, H.-L. Yip, T.-K. Lau, X. Lu, C. Zhu, H. Peng, P. A. Johnson, M. Leclerc, Y. Cao, J. Ulanski, Y. Li and Y. Zou, *Joule*, 2019, **3**, 1140-1151.

11. Q. Fan, W. Su, S. Chen, W. Kim, X. Chen, B. Lee, T. Liu, U. A. Méndez-Romero, R. Ma, T. Yang, W. Zhuang, Y. Li, Y. Li, T.-S. Kim, L. Hou, C. Yang, H. Yan, D. Yu and E. Wang, *Joule*, 2020, **4**, 658-672.

12. M. Qian, R. Zhang, J. Hao, W. Zhang, Q. Zhang, J. Wang, Y. Tao, S. Chen, J. Fang and W. Huang, *Adv. Mater.*, 2015, **27**, 3546-3552.

13. Z. Wan, J. Yang, Y. Liu, S. Wang, Y. Zhong, C. Li, Z. Zhang, G. Xing, S. Huettner, Y. Tao, Y. Li and W. Huang, Polym. Chem., 2017, **8**, 4729-4737.

14. Z. Xue, S. Wang, J. Yang, Y. Zhong, M. Qian, C. Li, Z. Zhang, G. Xing, S. Huettner, Y. Tao, Y. Li and W. Huang, npj Flex. Electron., 2018, **2**, 1.

15. X. Xu, K. Feng, Z. Bi, W. Ma, G. Zhang and Q. Peng, *Adv. Mater.*, 2019, **31**, 1901872.

16. R. Sun, T. Wang, Z. Luo, Z. Hu, F. Huang, C. Yang and J. Min, *Sol. RRL*, 2020, **4**, 2000156.

17. T. Wang, R. Sun, M. Shi, F. Pan, Z. Hu, F. Huang, Y. Li and J. Min, *Adv. Energy Mater.*, 2020, **10**, 2000590.

18. W. Jiang, R. Yu, Z. Liu, R. Peng, D. Mi, L. Hong, Q. Wei, J. Hou, Y. Kuang and Z. Ge, *Adv.*

Mater., 2018, **30**, 1703005.

19. X. Wang, Q. Sun, J. Gao, X. Ma, J. H. Son, S. Y. Jeong, Z. Hu, L. Niu, H. Y. Woo, J. Zhang and F. Zhang, *Sol. RRL*, 2021, **5**, 2100007.
20. X. Xu, K. Feng, Y. W. Lee, H. Y. Woo, G. Zhang and Q. Peng, *Adv. Funct. Mater.*, 2020, **30**, 1907570.
21. M. Jiang, H. Bai, H. Zhi, L. Yan, H. Woo, L. Tong, J. Wang, F. Zhang, Q. An, *Energy Environ. Sci.*, 2021, **14**, 3945-3953
22. Z. Chen, W. Song, K. Yu, J. Ge, J. Zhang, L. Xie, R. Peng and Z. Ge, *Joule*, 2021, DOI: 10.1016/j.joule.2021.06.017.
23. Z. Zhao, B. Liu, C. Xu, M. Liu, K. Yang, X. Zhang, Y. Xu, J. Zhang, W. Li and F. Zhang, *J. Mater. Chem. C*, 2021, **9**, 5349-5355.
24. Z. Hu, Z. Wang, Q. An, F. Zhang, *Sci. Bull.*, 2020, **65**,131–137.
25. P. Bi and X. Hao, *Sol. RRL*, 2019, **3**, 1800263.
26. J. Gao, X. Ma, C. Xu, X. Wang, J. H. Son, S. Y. Jeong, Y. Zhang, C. Zhang, K. Wang, L. Niu, J. Zhang, H. Y. Woo, J. Zhang and F. Zhang, *Chem. Eng. J.*, 2022, **428**, 129276.
27. S. M. Menke, N. A. Ran, G. C. Bazan and R. H. Friend, *Joule*, 2018, **2**, 25-35.
28. X. Ma, J. Wang, J. Gao, Z. Hu, C. Xu, X. Zhang and F. Zhang, *Adv. Energy Mater.,* 2020, **10**, 2001404.
29. Z. Hu, J. Wang, X. Ma, J. Gao, C. Xu, X. Wang, X. Zhang, Z. Wang, F. Zhang, *J. Mater. Chem. A,* 2021, **9**, 6797-6804.
30. M. Zhang, Z. Xiao, W. Gao, Q. Liu, K. Jin, W. Wang, Y. Mi, Q. An, X. Ma, X. Liu, C. Yang, L. Ding and F. Zhang, *Adv. Energy Mater.,* 2018, **8**, 1801968.

31. Z. Zhou, S. Xu, J. Song, Y. Jin, Q. Yue, Y. Qian, F. Liu, F. Zhang and X. Zhu, *Nat. Energy*, 2018, **3**, 952-959.

32. Y. Chen, P. Ye, Z. G. Zhu, X. Wang, L. Yang, X. Xu, X. Wu, T. Dong, H. Zhang, J. Hou, F. Liu and H. Huang, *Adv. Mater.*, 2017, **29**, 1603154.

33. K. Yang, J. Wang, Z. Zhao, Z. Zhou, M. Liu, J. Zhang, Z. He and F. Zhang, *ACS Appl. Mater. Interfaces*, 2021, **13**, 21565-21572.

34. R. Ma, T. Liu, Z. Luo, K. Gao, K. Chen, G. Zhang, W. Gao, Y. Xiao, T.-K. Lau, Q. Fan, Y. Chen, L.-K. Ma, H. Sun, G. Cai, T. Yang, X. Lu, E. Wang, C. Yang, A. K. Y. Jen and H. Yan, *ACS Energy Lett.*, 2020, **5**, 2711-2720.

35. H. Fu, C. Li, P. Bi, X. Hao, F. Liu, Y. Li, Z. Wang and Y. Sun, *Adv. Funct. Mater.*, 2019, **29**, 1807006.

36. Y. Cui, H. Yao, L. Hong, T. Zhang, Y. Tang, B. Lin, K. Xian, B. Gao, C. An, P. Bi, W. Ma and J. Hou, *Natl. Sci. Rev.*, 2020, **7**, 1239-1246.

37. K. Li, Y. Wu, Y. Tang, M. A. Pan, W. Ma, H. Fu, C. Zhan and J. Yao, *Adv. Energy Mater.*, 2019, **9**, 1901728.

38. X. Ma, A. Zeng, J. Gao, Z. Hu, C. Xu, J. Son, S. Jeong, C. Zhang, M. Li, K. Wang, H. Yan, Z. Ma, Y. Wang, H. Woo and F. Zhang, *Natl. Sci. Rev.,* 2021, **8**, nwaa305.

39. L. Zhang, N. Yi, W. Zhou, Z. Yu, F. Liu and Y. Chen, *Adv. Sci.*, 2019, **6**, 1900565.

40. Y. Wang, F. Wang, J. Gao, Y. Yan, X. Wang, X. Wang, C. Xu, X. Ma, J. Zhang and F. Zhang, *J. Mater. Chem. C*, 2021, **9**, 9892-9898

41. T. Yan, W. Song, J. Huang, R. Peng, L. Huang and Z. Ge, *Adv. Mater.*, 2019, **31**, 1902210.

42. W. Li, J. Cai, F. Cai, Y. Yan, H. Yi, R. S. Gurney, D. Liu, A. Iraqi and T. Wang, *Nano Energy*,

2018, **44**, 155-163.

43. B. Xiao, M. Zhang, J. Yan, G. Luo, K. Gao, J. Liu, Q. You, H.-B. Wang, C. Gao, B. Zhao, X. Zhao, H. Wu and F. Liu, *Nano Energy*, 2017, **39**, 478-488.
44. M. Liu, J. Wang, Z. Zhao, K. Yang, P. Durand, F. Ceugniet, G. Ulrich, L. Niu, Y. Ma, N. Leclerc, X. Ma, L. Shen and F. Zhang, *J. Phys. Chem. Lett.*, 2021, **12**, 2937-2943.
45. Z. Zhao, M. Liu, K. Yang, C. Xu, Y. Guan, X. Ma, J. Wang and F. Zhang, *Adv. Funct. Mater.*, 2021 **31**, 2106009.
46. T. Clarke, C. Lungenschmied, J. Peet, N. Drolet and A. Mozer, *Adv. Energy Mater.*, 2015, **5**, 1401345.
47. G. Perrier, R. de Bettignies, S. Berson, N. Lemaître and S. Guillerez, *Sol. Energy Mater Sol. Cells*, 2012, **101**, 210-216.
48. T. Kumari, S. M. Lee, K. C. Lee, Y. Cho and C. Yang, *Adv. Energy Mater.*, 2018, **8**, 1800616.
49. X. Ouyang, R. Peng, L. Ai, X. Zhang and Z. Ge, *Nat. Photonics*, 2015, **9**, 520-524.
50. Q. Fan, Q. An, Y. Lin, Y. Xia, Q. Li, M. Zhang, W. Su, W. Peng, C. Zhang, F. Liu, L. Hou, W. Zhu, D. Yu, M. Xiao, E. Moons, F. Zhang, T. D. Anthopoulos, O. Inganäs and E. Wang, *Energy Environ. Sci.*, 2020, **13**, 5017-5027.
51. Y. Ma, D. Cai, S. Wan, P. Yin, P. Wang, W. Lin and Q. Zheng, *Natl. Sci. Rev.*, 2020, **7**, 1886-1895.
52. Q. An, F. Zhang, W. Gao, Q. Sun, M. Zhang, C. Yang and J. Zhang, *Nano Energy*, 2018, **45**, 177-183.
53. X. Xu, L. Yu, H. Yan, R. Li and Q. Peng, *Energy Environ. Sci.*, 2020, **13**, 4381-4388.
54. L. Liu, Y. Kan, K. Gao, J. Wang, M. Zhao, H. Chen, C. Zhao, T. Jiu, A. K. Jen and Y. Li,

Adv. Mater., 2020, **32**, 1907604.

55. K. Yang, Z. Zhao, M. Liu, Z. Zhou, K. Wang, X. Ma, J. Wang, Z. He, F. Zhang, *Chem. Eng. J.,* 2022, **427**, 131802.

56. C. Xu, H. Chen, Z. Zhao, J. Gao, X. Ma, S. Lu, X. Zhang, Z. Xiao and F. Zhang, *J. Energy Chem.*, 2021, **57**, 610-617.

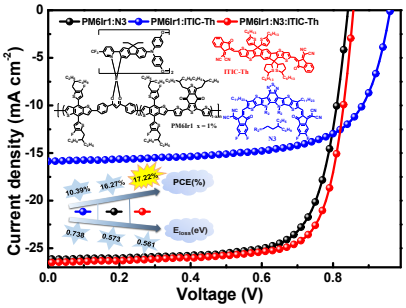

Ternary PSCs were fabricated with iridium-based polymer PM6Ir1 as donor, ITIC-Th and N3 as acceptors. The incorporation of ITIC-Th can effectively optimize the phase separation and molecular arrangement for efficient charge separation and transport in the ternary active layer, leading to the PCE enhancement from 16.27% to 17.22%.

Supporting information

Ternary polymer solar cells with iridium-based polymer PM6Ir1 as donor and N3:ITIC-Th as acceptors exhibiting over 17.2% efficiency

Shuping Zhang[a], Miao Zhang[a,c], Xuelin Wang[a], Chunyu Xu[a], Wenjing Xu[a], Jinhua Gao[a]*, Jian Wang[b], Wai-Yeung Wong[c,d]*, Jae Hoon Son[e], Sang Young Jeong[e], Han Young Woo[e], Fujun Zhang[a]*

a) School of Science, Beijing Jiaotong University, 100044, Beijing, China.

b) College of Physics and Electronic Engineering, Taishan University, 271021, Taian, China.

c) Department of Applied Biology and Chemical Technology and Research Institute for Smart Energy, The Hong Kong Polytechnic University, Hung Hom, Hong Kong, China.

d) The Hong Kong Polytechnic University Shenzhen Research Institute, 518057, Shenzhen, China.

e) Organic Optoelectronic Materials Laboratory, Department of Chemistry, College of Science, Korea University, 02841, Seoul, Republic of Korea.

Corresponding Email:

E-mail: jinhuagao@bjtu.edu.cn (JH), wai-yeung.wong@polyu.edu.hk (WY), fjzhang@bjtu.edu.cn (FJ)

Experimental section

Device Fabrication: The patterned indium tin oxide (ITO) coated glass substrates (sheet resistance 15 Ω/square) were consecutively cleaned in ultrasonic baths containing detergent, de-ionized water and ethanol, respectively. The cleaned ITO substrates were blow-dried by highly pure nitrogen gas and then treated by oxygen plasma for 1 min to improve its work function and cleanliness. Subsequently, poly (3,4-ethylenedioxythiophene): poly (styrene sulfonate) (PEDOT:PSS) (clevios PVP Al 4083, purchased from H.C. Starck co. Ltd.) solution was spin-coated to fabricate thin films on the cleaned ITO substrates by spin-coating method at 5000 round per minute (RPM)

for 40 s, and then annealed at 150 °C for 15 min in ambient condition. After annealing treatment, the ITO substrates coated with PEDOT:PSS films were transferred to a high-purity nitrogen-filled glove box for the fabrication of active layers. The PM6Ir1, N3 and ITIC-Th were dissolved in chlorobenzene to prepare 16 mg/ml blend solutions and 1-chloronaphthalene (CN) (0.5%, v/v) was added as the additive. The PM6Ir1 was synthesized by M. Zhang according to the following synthetic method. ITIC-Th and N3 were purchased from Solarmer Materials Inc and eFlexPV limited company, respectively. The proportions of N3:ITIC-Th are 1:0, 0.95:0.05, 0.9:0.1, 0.85:0.15, 0.7:0.3, 0:1 and the weight ratio of donor to acceptors is kept constant as 1:1.2. The blend solutions were spin-coated onto PEDOT:PSS films at 2800 RMP for 30 s in a high purity nitrogen-filled glove box to fabricate the active layers. Then, the active layers were annealed by CS_2 vapor for 20 s and then thermally annealed at 80 °C for 5 min. Afterwards, a PDIN cathode interlayer was spin-coated onto active layers at 5000 RPM for 30 s. Finally, 100 nm Ag was deposited by thermal evaporation with a shadow mask. The active area is approximately 3.8 mm^2, which is defined by the overlapping area of ITO anode and Ag cathode.

Synthetic method of PM6Ir1

Three monomers of (4,8-bis(5-(2-ethylhexyl)-4-fluorothiophen-2-yl)benzo[1,2-*b*:4,5-*b*']-dithiophene (BDT-F, 188.5 mg, 0.2 mmol) and 1,3-bis(thiophen-2-yl)-5,7-bis(2-ethyl-hexyl)benzo-[1,2-*c*:4,5-*c*']dithiophene-4,8-dione (BDD, 153.3 mg, 0.2 mmol) and bis[2-di(p-methoxyphenyl)-amino (9,9-diethylfluoren-2-yl)-5-(trifluoromethyl)pyridine][1,3-bis(4-bromophenyI)propane-1,3-dione]iridium(III)[1] (iridium complex, 3.5 mg, 0.002 mmol were added into a 25 mL Schlenk flask containing 15 mL of dry toluene. Under high-purity nitrogen atmosphere, $Pd(PPh_3)_4$ (20 mg, 0.02 mmol) was added. Then the reaction mixture was heated to reflux for 2 days. After that, the solution mixture after colling was poured into MeOH, and the precipitate was collected by filtration. Then, the polymer PM6Irl was collected as a dark solid after Soxhlet extraction with methanol, hexane, and chloroform for 24 h, respectively. Finally, the solid was dried under vacuum for 1 day and PM6Ir1 was

obtained with a 62% yield (152 mg).

The number average molecular weight (M_n) is 29.8 kDa and the polydispersity index (PDI) is 1.48 for terpolymer PM6Ir1, measured by gel permeation chromatography (GPC). Elemental analysis is performed to further confirm the PM6Ir1 structure and the result is listed as Anal. calcd. (%): C, 67.26; H, 6.59; N, 0.04; S, 20.26. Found (%): C, 66.71; H, 6.18; N, 0; S, 20.56. According to the thermogravimetric analysis (TGA) measurement shown in **Fig. S1a**, the decomposition temperatures (T_d) of terpolymer PM6Ir1 is 437 ℃ when its weight is reduced to 95% of the initial value. **Fig. S1b** exhibits the linearly fitted the inductively coupled plasma mass-spectrometry (ICP-MS) curves of iridium standard and polymer signal. According to the perfect linear fit of iridium standard signals with the coefficient of determination R^2 = 1.0, the measured concentration of iridium component is 1.093 ppb for terpolymer PM6Ir1, which further identify the existence of iridium component in polymer backbone.

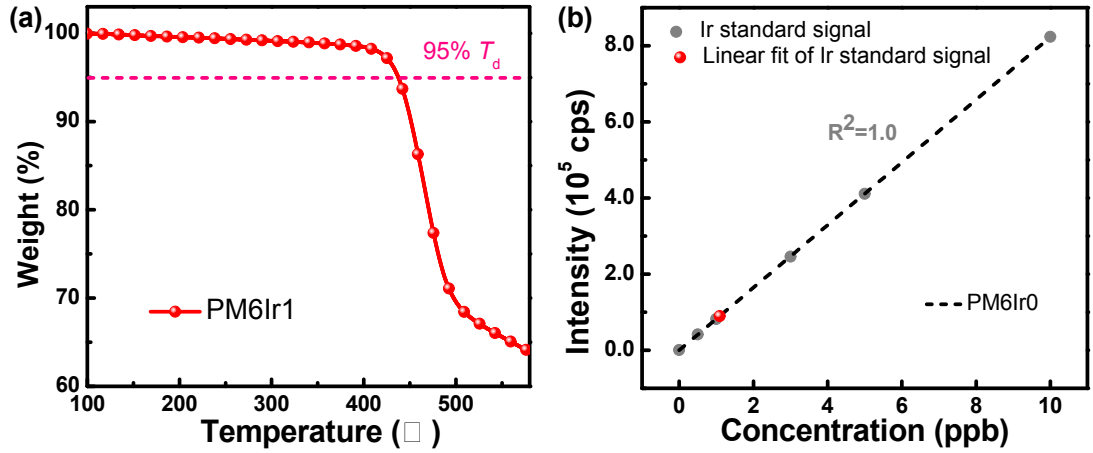

Fig. S1. (a) TGA plots of polymer donors with a heating rate of 10 ℃ min^{-1} under a N_2 atmosphere. (b) Linearly fitted ICP-MS curves of iridium standard and polymer PM6Ir1 signal.

Device Characterization: The current density-voltage (*J-V*) curves of all the organic solar cells were measured by a Keithley 2400 unit in a high-purity nitrogen-filled glove box. The AM 1.5G irradiation was provided by an XES-40S2 (SAN-EI ELECTRIC Co. Ltd) solar simulator (AAA grade, 70×70 mm^2 photobeam size) with light intensity of 100 mW/cm^2, which was calibrated by standard silicon solar cells (purchased from Zolix INSTRUMENTS CO. LTD). The external quantum efficiency (EQE) spectra of

organic solar cells were measured in air by a Zolix Solar Cell Scan 100. The ultraviolet-visible (UV-Vis) absorption spectra of neat and blend films were obtained using a Shimadzu UV-3101 PC spectrometer. Photoluminescence (PL) spectra of neat and blend films were measured by a HORIBA Fluorolog®-3 spectrofluorometer system. Electrochemical impedance spectroscopy (EIS) was measured by a ZAHNER CIMPS electrochemical workstation, Germany. Transmission electron microscopy (TEM) images of active layers were obtained by a JEOL JEM-1400 transmission electron microscope operated at 80 kV. Grazing incidence wide angle X-ray scattering (GIWAXS) measurements were accomplished at PLS-II 9A U-SAXS beamline of the Pohang Accelerator Laboratory in Korea.

The space charge limited current (SCLC) method was employed to investigate the influence of incorporating ITIC-Th on charge mobility in active layers. The structure of electron-only devices is ITO/ZnO/active layer/PDIN/Al and the structure of hole-only devices is ITO/PEDOT:PSS/active layer/MoO_3/Ag. ZnO thin films were fabricated on the cleaned ITO substrates by spin-coating method at 4000 RPM for 30 s, and then annealed at 150 °C for 30 min in air conditions. The thickness of ZnO films is about 30 nm. After annealing treatment, the ITO substrates coated ZnO films were transferred to a high-purity nitrogen-filled glove box to fabricate active layers. The fabrication conditions of the active layer films are same with those for the solar cells. After that, the MoO_3/Ag (10 nm/100 nm) films were deposited by thermal evaporation with a shadow mask under 10^{-4} Pa. The charge mobility was calculated according to the space charge limited current (SCLC) method. The hole and electron mobility can be calculated from the Mott-Gurney equation with Poole-Frenkel correction as the followings:

$$J = \frac{9}{8}\varepsilon_0\varepsilon_r\mu\frac{V^2}{d^3}exp\left[0.89\gamma\sqrt{\frac{V}{d}}\right]$$

Here, ε_r is dielectric constant of organic materials, ε_0 is the free space permittivity, μ is charge mobility, V is the applied voltage, and d is the active layer thickness, γ is the field enhancement factor of a Poole–Frenkel type mobility.

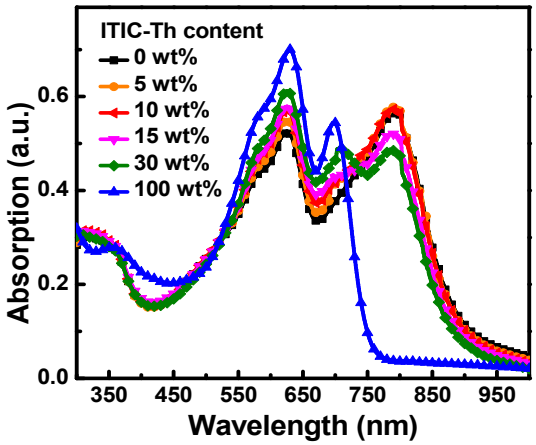

Fig. S2. Absorption spectra of blend films with different ITIC-Th content.

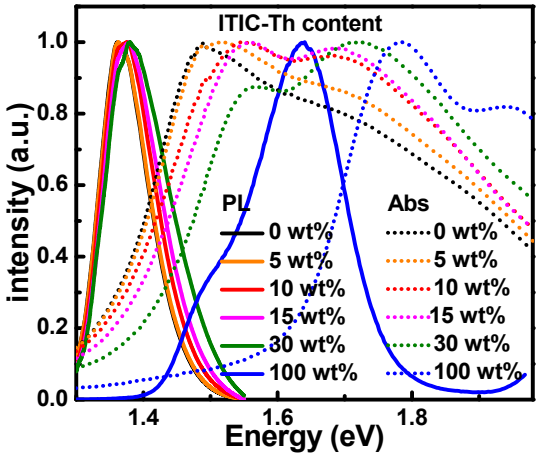

Fig. S3. The normalized absorption spectra and PL spectra of neat and blend acceptor films.

Photocurrent density (J_{ph}) dependence on effective voltage (V_{eff}) of typical PSCs were investigated. The J_{ph} is defined as $J_{ph} = J_L - J_D$, in which J_L and J_D represent the current densities under illumination and dark conditions, respectively. The V_{eff} is defined as $V_{eff} = V_0 - V_{bias}$, in which V_0 represents the voltage at $J_{ph} = 0$ mA cm^{-2} and V_{bias} represents the applied voltage bias. Assumed that the exciton dissociation efficiency (η_{diss}) and charge collection efficiency (η_{coll}) are very close to 100% under large V_{eff} of 4 V, the J_{ph} at $V_{eff} = 4$ V is defined as the saturated current density (J_{sat}). The η_{diss} and η_{coll} can be calculated according to the formula of $\eta_{diss} = J_{ph}^{*}/J_{sat}$ and $\eta_{coll} = J_{ph}^{\#}/J_{sat}$, the J_{ph}^{*} and $J_{ph}^{\#}$ refer to the J_{ph} under short-circuit condition and maximal-power-output condition, respectively. The detailed values of corresponding PSCs are listed in Table S1.

Table S1. The key parameters of the optimized binary and ternary PSCs.

Blend films [a)]	J_{ph}^{*} (mA cm^{-2})	$J_{ph}^{\#}$ (mA cm^{-2})	J_{sat} (mA cm^{-2})	J_{ph}^{*}/J_{sat} (%)	$J_{ph}^{\#}/J_{sat}$ (%)
PM6Ir1:N3	26.13	23.84	27.64	94.55	86.24
PM6Ir1:N3:ITIC-Th	26.53	24.36	27.84	95.28	87.47
PM6Ir1:ITIC-Th	15.87	13.48	17.35	91.47	77.69

[a)] J_{ph}^{*} under short-circuit condition, $J_{ph}^{\#}$ under maximal-power-output condition.

Table S2. The key parameters of the optimized binary and ternary PSCs.

ITIC-Th content (wt%)	R_s (Ω)	R_{trans} (Ω)	C (nF)	R_{rec} (Ω)	CPE_P	CPE_T (nF)
0	29.6	59.5	4.14	62.4	0.910	15.1
10	33.1	54.9	13.3	65.2	0.955	13.3
100	23.3	189	1.83	102	0.859	7.96

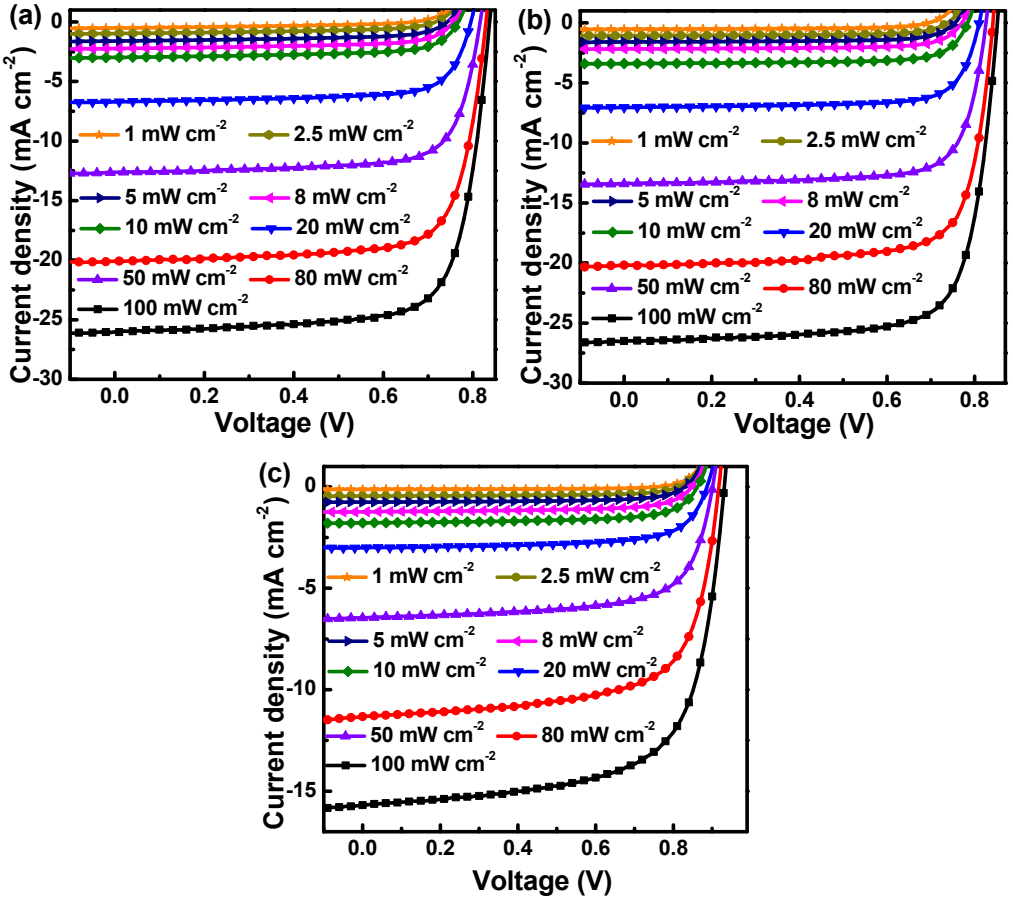

Fig. S4. *J-V* curves of the PSCs under AM 1.5G illumination with light intensity of 100, 80, 50, 25, 10, 5, 2.5, 1 mW/cm^2, respectively: (a) N3 based binary PSCs, (b) optimized

ternary PSCs, (c) ITIC-Th based binary PSCs.

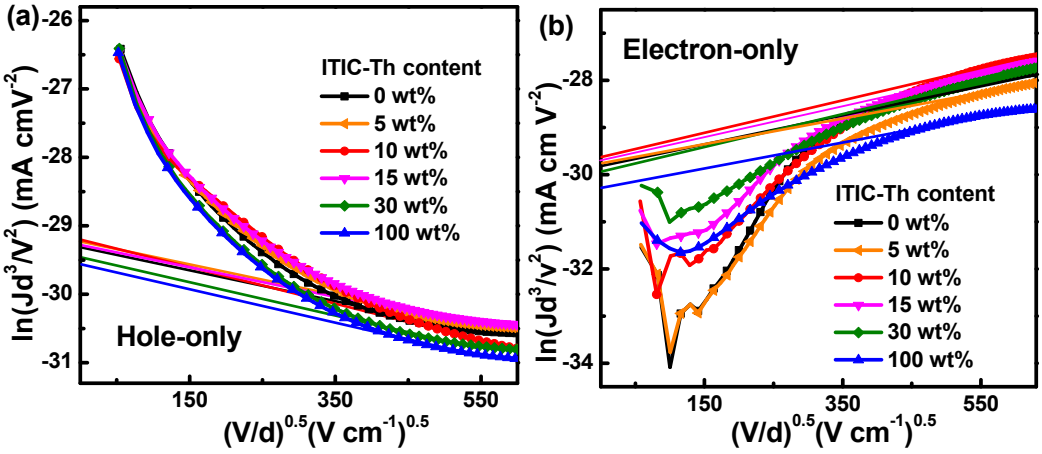

Fig. S5. The $\ln(Jd^3/V^2)$ versus $(V/d)^{0.5}$curves of (a) hole-only devices and (b) electron-only devices.

Table S3. The μ_h, μ_e and μ_h/μ_e in the OSCs with different ITIC-Th contents in the acceptor mixture.

ITIC-Th content (wt%)	μ_h ($cm^2\ V^{-1}\ s^{-1}$)	μ_e ($cm^2\ V^{-1}\ s^{-1}$)	μ_h/μ_e
0	6.46×10^{-4}	3.98×10^{-4}	1.62
5	6.63×10^{-4}	4.28×10^{-4}	1.55
10	6.97×10^{-4}	4.59×10^{-4}	1.52
15	6.56×10^{-4}	4.29×10^{-4}	1.60
30	5.37×10^{-4}	3.32×10^{-4}	1.88
100	4.84×10^{-4}	2.32×10^{-4}	2.08

1. X. Liu, B. Yao, Z. Zhang, X. Zhao, B. Zhang, W.-Y. Wong, Y. Cheng and Z. Xie, *J. Mater. Chem. C*, 2016, 4, 5787-5794.